Eur. Phys. J. D **46**, 267–279 (2008)
DOI: 10.1140/epjd/e2007-00317-0

THE EUROPEAN PHYSICAL JOURNAL D

Electron impact excitation of 2p and 3p states of hydrogen at intermediate energies

M.Z.M. Kamali[1], K. Ratnavelu[2,a], and Y. Zhou[3]

[1] Centre for Foundation Studies in Science, University of Malaya, Kuala Lumpur, Malaysia
[2] Institute of Mathematical Sciences, University of Malaya, Kuala Lumpur, Malaysia
[3] Institute of Atomic and Molecular Physics, Jilin University, 130012 Changchun, P.R. China

Received 11 July 2007 / Received in final form 5 October 2007
Published online 28 November 2007

Abstract. The recent theoretical work by Bartlett et al. [J. Phys. B **38**, L95 (2005)] and the latest measurements on the reduced Stokes parameters $\overline{P}_1$, $\overline{P}_2$ and $\overline{P}_3$ for 54.4 eV electron impact excitation of the $2p$ state atomic hydrogen by Williams and Mikosza [J. Phys. B **39**, 4113 (2006)] has motivated the present work. A coupled-channel-optical calculation with 9 and 12 atomic states supplemented with the continuum optical potentials for the stronger coupling channels has been performed. The calculated $n = 2$ and $n = 3$ differential cross sections and the reduced Stokes parameters are comparable with the *state-of-the art* calculations. There is closer agreement between the present calculations and the experimental measurements for the reduced Stokes parameters $\bar{P}_1$ and $\bar{P}_3$ in the $n = 2p$ excitation at 54.4 eV. The present CCO calculations also display good accord with the limited experimental data for the reduced Stokes parameters in the $n = 3p$ excitation.

PACS. 34.10.+x General theories and models of atomic and molecular collisions and interactions – 34.80.-i Electron scattering – 34.80.Dp Atomic excitation and ionization by electron impact

1 Introduction

The present work was initially motivated as an interest of this group to probe for the similarities and differences between the physics of positron-hydrogenic-type atom and electron-hydrogenic-type atom [3–6] at intermediate energies. With the advent of recent experimental measurements [2,7–12] on the electron impact excitation of $2p$ and $3p$ states of hydrogen atom has provided us an interesting challenge to test the coupled-channel-optical calculation (CCO) [13] with the best available theoretical calculation [1,14,15] and these experimental measurements.

The present *state of the art* theoretical methods such as the propagating exterior scaling complex (PECS) [1], the convergent close-coupling-Laguerre (CCC-L) [14], the close-coupling of Wang et al. (CC17) [15] and the box-based convergent close-coupling method (CCC-B) [16], have reached a high level of accuracy in predicting total and differential cross sections (DCS) for electron scattering from atomic hydrogen. The CC17 had utilized a large 17-state target basis set that consisted of seven exact atomic states ($1s$, $2s$, $2p$, $3s$, $3p$, $3d$ and $4f$) together with ten pseudostates (5 s-like, 3 p-like and 2 d-like). They reported the DCS, and the angular correlation parameters λ, R and I at energies ranging from 16 eV to 100 eV that showed good agreement with the experimental measurements for some of these physical quantities.

The CCC-L method [14] which employs the orthogonal basis of Laguerre functions to represent the target states has been very successful in studying the electron-hydrogen scattering system. The benefit of using this method is that the convergence can be achieved by expanding the basis size without suffering from the linear dependence problems associated with the ordinary Slater type basis sets in the limit of large expansions. Further improvements by Bray et al. [16] were implemented in the CCC-B method. In this variant of the CCC method, the Laguerre basis was replaced by the box-based eigenstates to find the eigenstate $\phi(r)$ of the Hamiltonian. The DCS calculated with the CCC-B method was in close agreement with the CCC-L method.

The latest implementation (PECS) of the exterior complex scaling method (ECS) (Rescigno et al. [17]) was reported by Bartlett et al. [18] and Bartlett and Stelbovics [19], is considered the most complete method to solve the non-relativistic time-independent scattering problem. The propagation technique was used originally by Poet [20] to solve the Temkin-Poet [21,22] model for e-H ionization. This technique reduces significantly the computational complexity in the ECS method. In their recent work [1], both the PECS and CCC-B showed

[a] e-mail: kuru052001@gmail.com

excellent agreement with the CCC-L method for the three reduced Stokes parameters by Williams and Mikosza [2] and thus adding further controversy to the measurements of the $\overline{P}_3$ parameter data of Gradziel and O'Neill [7] and that of Chormaic et al. [25].

The early measurements of the 54.4 eV e-H($2p$) angular correlation parameters started in the 1980's [23,24]. With technological improvements over the last two decades, we have seen an array of measurements [2,7,9,10,25] that have reported either the angular correlation or reduced Stokes parameters for the electron impact excitation of H($2p$) at 54.4 eV. The difficulties in detecting the outgoing electron in coincidence with the $2p$ photon are very challenging and these measurements are also very vital as they provide extra information from the collision process.

The theoretical challenges in describing the details of the collision process particularly concerning the excited state charge cloud plays a vital role in gauging the quality of the method [26–28]. Besides the $2p$ excitation measurements of the reduced Stokes parameters, there has also been limited measurement for these parameters in the $3p$ excitation [29,30]. Thus in view of the recent developments, it seemed timely that a CCO calculation be attempted.

In this paper, the present CCO calculations are aimed at providing a comparative view of the DCS and the reduced Stokes parameters for $2p$, $3p$ excitation at 54.4 eV and other intermediate energies with other theoretical calculations.

2 Theory

When an electron is bombarded towards a hydrogen atom in its ground state, several classes of reactions are possible:

1. elastic
$$e^- + \mathrm{H}\,(1s) \rightarrow e^- + \mathrm{H}(1s);$$
2. inelastic
$$e^- + \mathrm{H}\,(1s) \rightarrow e^- + \mathrm{H}\,(nl \neq 1s) \quad \text{(atom excitation)};$$
3. reactions
$$e^- + \mathrm{H}\,(1s) \rightarrow e^- + e^- + \mathrm{H}^+ \quad \text{(ionization)}.$$

The Schrödinger equation for electron-hydrogen system is given as

$$\left(-\frac{1}{2}\nabla_1^2 - \frac{1}{2}\nabla_2^2 - \frac{1}{r_1} - \frac{1}{r_2} + \frac{1}{r_{12}} - E\right)\Psi(\mathbf{r}_1, \mathbf{r}_2) = 0 \tag{1}$$

where $\mathbf{r}_1$ and $\mathbf{r}_2$ represent the coordinate of e^- and incident e^- with respect to the proton, respectively. The momentum space Lippmann-Schwinger equations for an electron with momentum $\mathbf{k}$ incident on hydrogen atom in state ψ_α (atomic units are assumed throughout) are

$$\langle \mathbf{k}'\psi_{\alpha'}|T|\mathbf{k}\psi_\alpha\rangle = \langle \mathbf{k}'\psi_{\alpha'}|V^{(Q)}|\mathbf{k}\psi_\alpha\rangle + \sum_{\alpha''}\int d^3k'' \frac{\langle \mathbf{k}'\psi_{\alpha'}|V^{(Q)}|\mathbf{k}''\psi_{\alpha''}\rangle\langle \mathbf{k}''\psi_{\alpha''}|T|\mathbf{k}\psi_\alpha\rangle}{\left(E^{(+)} - \varepsilon_{\alpha''} - \frac{1}{2}k''^2\right)}. \tag{2}$$

The optical potential $V^{(Q)}$ represents the first-order static-exchange potential together with a non-local complex polarization term. In this complex polarization term, we have the virtual and real excitations of the Q-space which includes the target continuum and the remainder of the discrete channels that are not explicitly coupled in the coupled-channels calculation.

For the derivation of the optical potential, the Feshbach projection operator P and Q are used to decompose the whole space of target wave function into a subspace of wavefunction $P\Psi$. P-space describes the finite set of the discrete channels considered including the ground state while Q-space includes the continuum and the remaining discrete states that are not explicitly coupled in the coupled-channel calculation. The projection operators are defined as

$$P = \sum_{i\in P} |\psi_i\rangle\langle\psi_i| \tag{3}$$

$$Q = \sum_{j\in Q} |\psi_j\rangle\langle\psi_j|\,. \tag{4}$$

The optical potential allows only for discrete states and the continuum of H. From the projection operators, we have the following properties of P and Q operators

$$\begin{aligned} Q &= 1 - P & Q^{-1}Q &= 1 \\ PQ &= QP = 0 & & \\ P^2 &= P & Q^2 &= Q. \end{aligned} \tag{5}$$

All the equations below is given in operator form. The Schrödinger equation is written as

$$E - K - v = 0 \tag{6}$$

where $K = K_1 + K_2$ and $v = v_1 + v_2 + v_3$. By using the properties of P and Q in (5) into the Schrödinger equation (6), we obtain the following:

$$\sum_{\alpha'}\langle\psi_\alpha|(E-K-v)(P+Q)|\psi_{\alpha'}\rangle F_{\alpha'} = 0 \tag{7}$$

$$\Rightarrow \begin{cases} \sum_{\alpha'}\langle\psi_\alpha|P(E-K-v)(P+Q)|\psi_{\alpha'}\rangle F_{\alpha'} = 0 \\ \sum_{\alpha'}\langle\psi_\alpha|Q(E-K-v)(P+Q)|\psi_{\alpha'}\rangle F_{\alpha'} = 0 \end{cases} \tag{8}$$

$$\Rightarrow \begin{cases} \sum_{\alpha'}\langle\psi_\alpha|P(E-K-v)P|\psi_{\alpha'}\rangle F_{\alpha'} \\ \quad + \sum_{\alpha'}\langle\psi_\alpha|P(E-K-v)Q|\psi_{\alpha'}\rangle F_{\alpha'} = 0 \\ \sum_{\alpha'}\langle\psi_\alpha|Q(E-K-v)P|\psi_{\alpha'}\rangle F_{\alpha'} \\ \quad + \sum_{\alpha'}\langle\psi_\alpha|Q(E-K-v)Q|\psi_{\alpha'}\rangle F_{\alpha'} = 0 \end{cases} \tag{9}$$

$$\Rightarrow \begin{cases} \sum_{\alpha'}\langle\psi_\alpha|P(E-K-v)P|\psi_{\alpha'}\rangle F_{\alpha'} \\ \quad + \sum_{\alpha'}\langle\psi_\alpha|P(E-K)Q|\psi_{\alpha'}\rangle F_{\alpha'} \\ \quad = \sum_{\alpha'}\langle\psi_\alpha|PvQ|\psi_{\alpha'}\rangle F_{\alpha'} \\ \sum_{\alpha'}\langle\psi_\alpha|Q(E-K)P|\psi_{\alpha'}\rangle F_{\alpha'} \\ \quad + \sum_{\alpha'}\langle\psi_\alpha|Q(E-K-v)Q|\psi_{\alpha'}\rangle F_{\alpha'} \\ \quad = \sum_{\alpha'}\langle\psi_\alpha|QvP|\psi_{\alpha'}\rangle F_{\alpha'} \end{cases}. \tag{10}$$

Since P and Q-space are necessarily different and orthogonal, we have the following relationship:

$$\langle\psi_\alpha|P(E-K)Q|\psi_{\alpha'}\rangle = 0$$

or

$$\langle\psi_\alpha|Q(E-K)P|\psi_{\alpha'}\rangle = 0. \quad (11)$$

Substituting equation (9) inside (11), we obtain:

$$\Rightarrow \begin{cases} \sum\limits_{\alpha'}\langle\psi_\alpha|P(E-K-v)P|\psi_{\alpha'}\rangle F_{\alpha'} = \sum\limits_{\alpha'}\langle\psi_\alpha|PvQ|\psi_{\alpha'}\rangle F_{\alpha'} \\ \sum\limits_{\alpha'}\langle\psi_\alpha|Q(E-K-v)Q|\psi_{\alpha'}\rangle F_{\alpha'} = \sum\limits_{\alpha'}\langle\psi_\alpha|QvP|\psi_{\alpha'}\rangle F_{\alpha'} \end{cases} \quad (12)$$

or

$$\Rightarrow \begin{cases} P(E-K-v)P = PvQ \\ Q(E-K-v)Q = QvP \end{cases}.$$

The second equation from equation (12) can be written as

$$Q\psi_{\alpha'} = Q\frac{1}{Q(E-K-v)Q}QvP\psi_{\alpha'}. \quad (13)$$

Substituting equation (13) into the first equation of (12), we have

$$P(E-K-v)P\psi_{\alpha'} = PvQ\frac{1}{Q(E-K-v)Q}QvP\psi_{\alpha'}. \quad (14)$$

Since v_2 does not connect the P and Q spaces, equation (14) can be written as

$$P(E-K-v_1-v_2-v_3)P\psi_{\alpha'} = P(v_1+v_3)Q\frac{1}{Q(E-K-v)Q}Q(v_1+v_3)P\psi_{\alpha'}$$

$$P(E-K-v_2)P\psi_{\alpha'} = P(v_1+v_3)P\psi_{\alpha'} + P(v_1+v_3)Q\frac{1}{Q(E-K-v)Q}Q(v_1+v_3)P\psi_{\alpha'}. \quad (15)$$

From equation (15), we can define the optical potential $V^{(Q)}$ as

$$V^{(Q)} = v_1+v_3+(v_1+v_3)Q\frac{1}{Q(E-K-v)Q}Q(v_1+v_3). \quad (16)$$

The second term of the optical potential $V^{(Q)}$ formula is called the complex non-local polarization potential $W^{(Q)}$ and $V^{(Q)}$ can be simplified as

$$V^{(Q)} = V + W^{(Q)}. \quad (17)$$

The Green function can be written in a spectral representation and is given as

$$\frac{1}{Q(E-K-v)Q} = Q\sum_n \left|\Psi_n^{(-)}\right\rangle \frac{1}{E-E_n}\left\langle\Psi_n^{(-)}(q)\right| Q. \quad (18)$$

The spectral index n, is a discrete notation for the continuum and defines the asymptotic partition of the 3-body system into bound or ionized states and specifies the quantum numbers and momenta within each partition. We will assume that the state vectors of the Q space are plane waves i.e. v_3 is diagonal in Q space by making the weak-coupling approximation [31]. This is done to make the approximation that the Green's function is diagonal in Q space. The optical potential can be written explicitly by substituting equation (3) and (4) into (16) giving

$$V^{(Q)} = (v_1+v_3) + \sum_n\sum_{m\in Q}(v_1+v_3)\left|\psi_m\right\rangle\left\langle\psi_m\right|\left\langle\Psi_n^{(-)}\right\rangle \times \frac{1}{E-E_n}\langle\Psi_n^{(-)}|\psi_m\rangle\langle\psi_m|(v_1+v_3). \quad (19)$$

The theoretical details of the coupled-channel optical potential (CCO) can be found in the work of McCarthy and Stelbovics [13].

The following physical observables can be calculated for the corresponding T-matrix elements:

The differential cross section for scattering from channel j to i at an angle θ is

$$\frac{d\sigma_{ij}}{d\Omega} = (2\pi)^4\frac{k_i\hat{S}^2}{k_j\hat{l}^2}\sum_{m,m'}|\langle k_i;\, n'l'm'|T|nlm;\, k_j\rangle|^2. \quad (20)$$

The three angular correlation parameters for the $2p$ and $3p$ states of hydrogen are:

$$\lambda = \frac{\langle|a_0|^2\rangle}{\sigma_m} \qquad R = \frac{\mathrm{Re}\langle a_1a_0^*\rangle}{\sigma_m} \qquad I = \frac{\mathrm{Im}\langle a_1a_0^*\rangle}{\sigma_m}, \quad (21)$$

where σ_m is the differential cross section and a_m is the complex amplitude for the excitation of the $2p_m$ or $3p_m$ states. The $\langle\ \rangle$ represents the spin average of the product of two scattering amplitudes. These angular correlation parameters and the reduced Stokes parameters for the $2p$ and $3p$ excitation are related by

$$\overline{P}_1 = 2\lambda - 1 \qquad \overline{P}_2 = -2\sqrt{2}R \qquad \overline{P}_3 = 2\sqrt{2}I. \quad (22)$$

In this work, the following calculations for the CCO calculations were performed:

- CCO12: 12 hydrogen states ($1s$, $2s$, $2p$, $3s$, $3p$, $3d$, $4s$, $4p$, $4d$, $5s$, $5p$, $5d$) with continuum optical potentials for the $1s$–$1s$, $1s$–$2s$, $1s$–$2p$, $1s$–$3s$, $1s$–$3p$, $1s$–$4s$, $1s$–$4p$, $1s$–$5s$ and $1s$–$5p$ were used;
- CCO9: 9 hydrogen states ($1s$, $2s$, $2p$, $3s$, $3p$, $3d$, $4s$, $4p$, $4d$) with continuum optical potentials for the $1s$–$1s$, $1s$–$2s$, $1s$–$2p$, $1s$–$3s$, $1s$–$3p$, $1s$–$4s$ and $1s$–$4p$ were used.

3 Results and discussions

3.1 Differential cross sections for n = 2p, 3p excitation

3.1.1 54.4 eV

In Figures 1a and 1b, the DCS for the excitation of the $n = 2p$ and $3p$ states at 54.4 eV are depicted with the available experimental data of Williams [24] and Williams et al. [12]. The quality of the predicted DCS among the

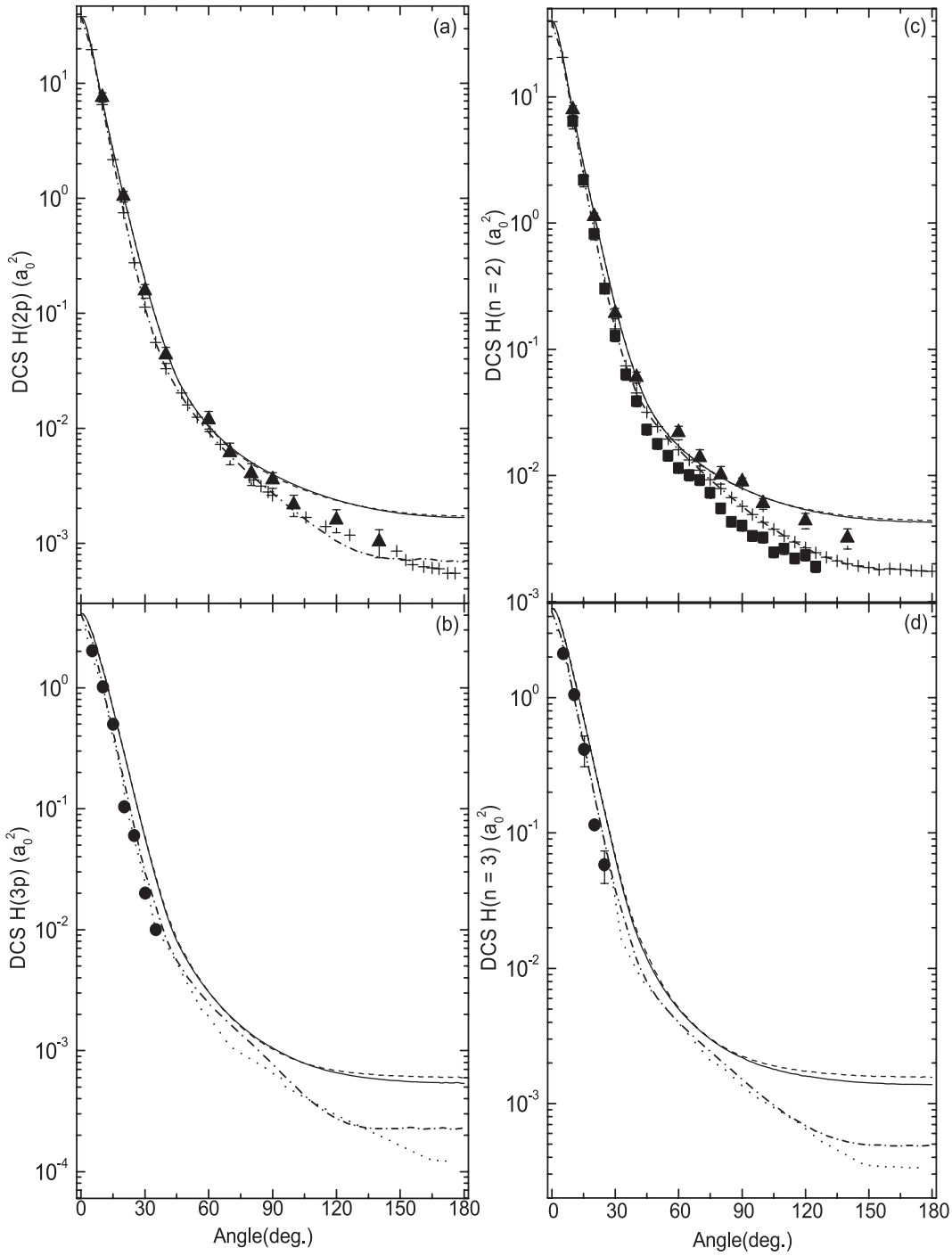

Fig. 1. The DCS for: (a) H($2p$) excitation, (b) H($3p$) excitation, (c) H($1s$) → H($2s + 2p$) excitation, (d) H($1s$) → H($3s + 3p$) excitation at 54.4 eV. Theoretical data: (——) CCO12, (- - - -) CCO9, (- · - · -) CC17, (+) CCC-L, (· · ·) PECS; experimental data: (▲) Williams [24], (■) Khakoo et al. [11], (●) Williams et al. [12].

various theories is very encouraging and suggests that the description of the physics of this scattering system may be complete. In the graphs, the reported PECS data is only shown for the H($3p$) and H($3s + 3p$) excitation. But it must be mentioned that in a recent report [1] PECS shows excellent agreement with the CCC variants for this scattering system.

In Figure 1a, the overall agreement between the Williams data [24] and the CCC-L and CC17 for the $n = 2p$ excitation is quite good. Even with its limited basis set, the present CCO method is in good accord with the CCC-L and the CC17 for this process except for the scattering region beyond 90°. The qualitative features preserved in all the calculations at forward and middle-angle

scattering suggests that from the large scale CCC-L to the smaller order CCO models are able to accommodate the physics of scattering at this energy. The differences only start emerging at the backward scattering angles where the high-energy approximations used in the CCO method may explain the differences with the CCC and CC17. However, the convergence between the CCO9 and CCO12 suggests the short-range correlation effects such as the exchange approximation in the optical potential may also be a more plausible reason for the differences in large-angle scattering.

In Figure 1b, the present CCO calculations for $n = 3p$ are lying slightly higher than the PECS and CC17 for most of the angles studied with better agreement at forward scattering angles below 20°. There is good agreement with the only experimental measurement of Williams [12] for angles below 20°.

In comparing further the quality of the CCO calculations for $n = 2s + 2p$ and $n = 3s + 3p$ excitation at 54.4 eV in Figures 1c and 1d respectively shows that the qualitative and quantitative agreement can be considered as fairly good over most of the forward and middle angle scattering. In fact, the CCO12 differential cross sections lies within Khakoo et al.'s experimental data [11] upto about 75° and with Williams data [24] to about 120°. This can be observed too for the $n = 3s+3p$ DCS in Figure 1d, where all theories and experiment [12] are indistinguishable in the forward scattering but there are some differences emerging at middle and backward angles. It seems that the physics of the scattering system is being well accommodated by the present CCO within its limitations.

Thus, there is enough evidence to suggest that the convergence gap between these theories and experiments are getting even smaller.

3.1.2 20 eV, 35 eV and 100 eV

Since there are some experimental data and a number of theoretical calculated DCS at some energies other than 54.4 eV, a comparative view is also presented here for the following: H($2p$), $n = 2$ (summed $2s$ and $2p$), H($3p$) and $n = 3$ (summed $3s$ and $3p$).

The DCS for H($2p$) transition at 20, 35 and 100 eV are shown in Figures 2a–2c. Generally, the present results show fair accord with other theories for forward and middle angle scattering in all the energies except at 20 eV. At higher angles, the CCO's DCS seems to be larger than those of the CC17 and the CCC. The large differences observed at higher scattering angles decreases as the incident energy increases. This is possibly due to the fact that the high-energy approximations used in the CCO models would be valid at higher energies.

Figures 3a–3c shows the present results for the $n = 2$ (summed $2s$ and $2p$) DCS, together with the available experimental data [11,24,32]. In order not to make the figures cluttered, only the CCO12 data are depicted. At 20 eV (Fig. 3a), the DCS is clearly overestimated by the CCO12 for all angles larger than 30°. But it must be also noted that the Williams [24] data is larger than the Grafe et al. [32] data above 120°. The differences between the CCO12 and other theoretical data are very large suggesting that the quality of the CCO at this low intermediate energy is clearly compromised by the high-energy approximations used in the optical model.

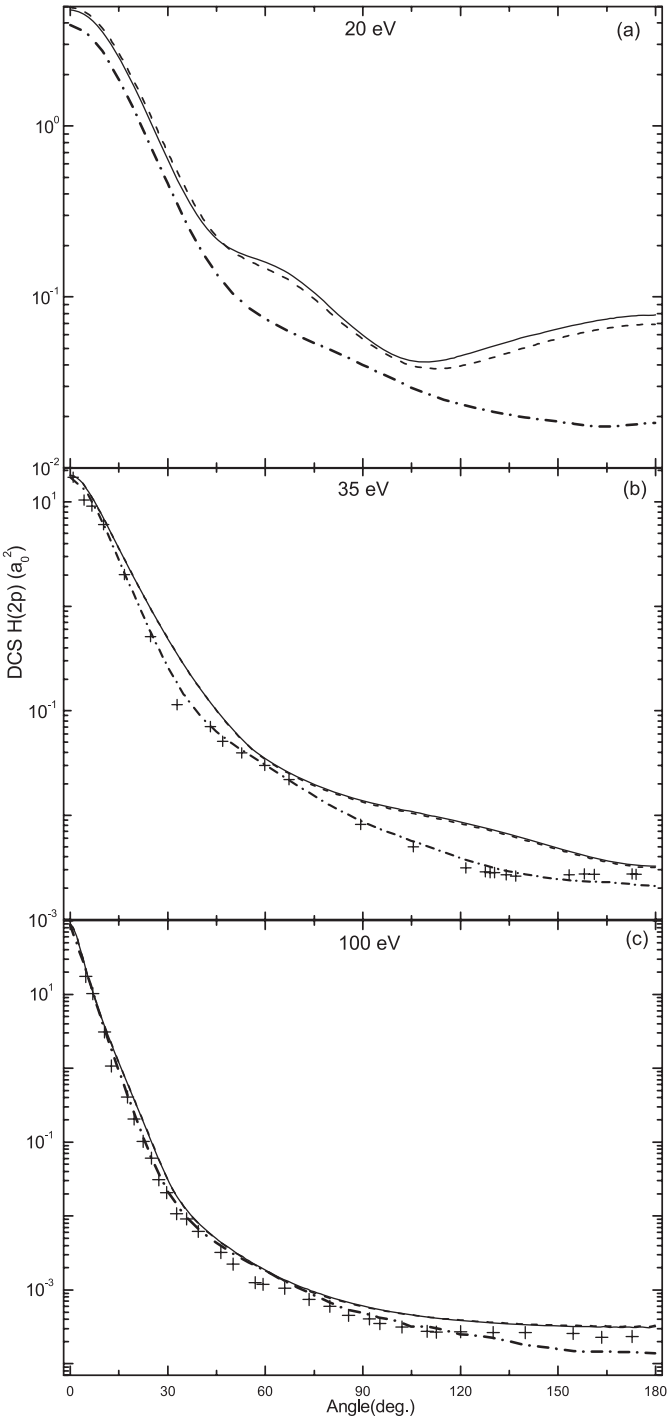

Fig. 2. The DCS for H($2p$) excitation at 20, 35 and 100 eV. Theoretical data: (——) CCO12, (- - - -) CCO9, (- · - · -) CC17, (+) CCC-L.

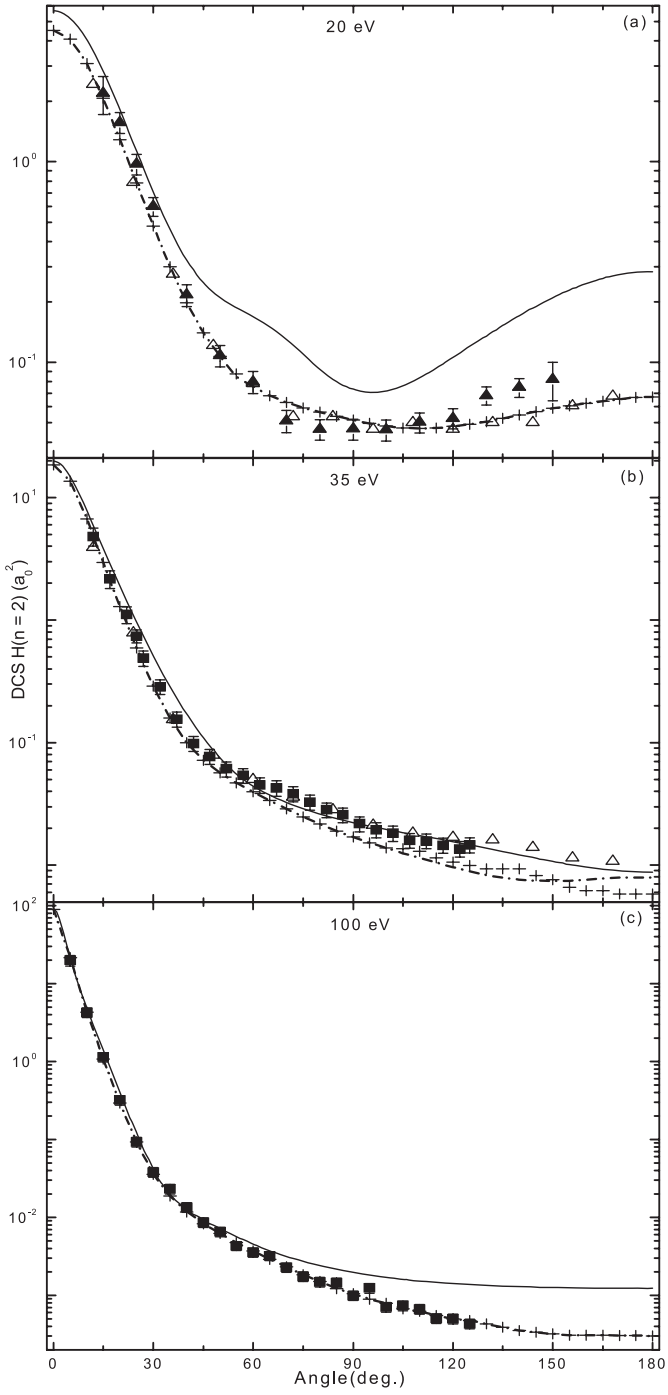

Fig. 3. The DCS for H($1s$) → H($2s + 2p$) excitation at 20, 35 and 100 eV. Theoretical data: similar to Figure 2. Experimental data: (■) Khakoo et al. [11], (▲) Williams [24], (△) Grafe et al. [32].

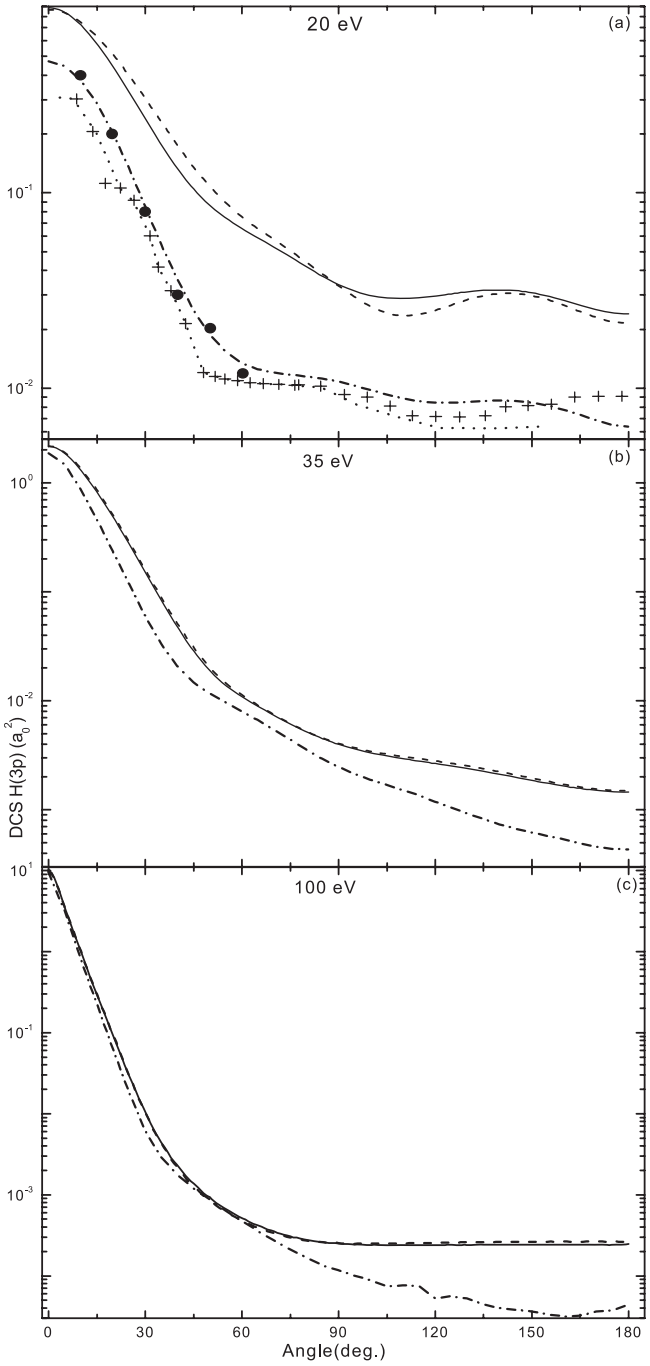

Fig. 4. The DCS for H($3p$) excitation at 20, 35 and 100 eV. Theoretical data: (——) CCO12, (----) CCO9, (-·-·-) CC17, (+) CCC-L, (···) PECS; experimental data: (●) Williams et al. [12].

However, at the incident energy of 35 eV (Fig. 3b), present DCS are in good accord with the measured data of Grafe and co-workers. The CCO also is in excellent agreement with the measurements done by Khakoo et al. [11] at middle and backward angles compared to those calculated by the CCC or the CC17 method. At 100 eV (Fig. 3c), there is better agreement but there is still some overestimation at backward angles in comparison with the experimental data [11].

Figures 4a–4c illustrates the DCS for $3p$ at 20, 35 and 100 eV. Again, at 20 eV, the CCO models overestimates the cross section for all the angles here, compared to other theories (CCC, CC17 and PECS). As the incident energy increases these differences are reduced especially at forward angles. However, there are still some discrepancies

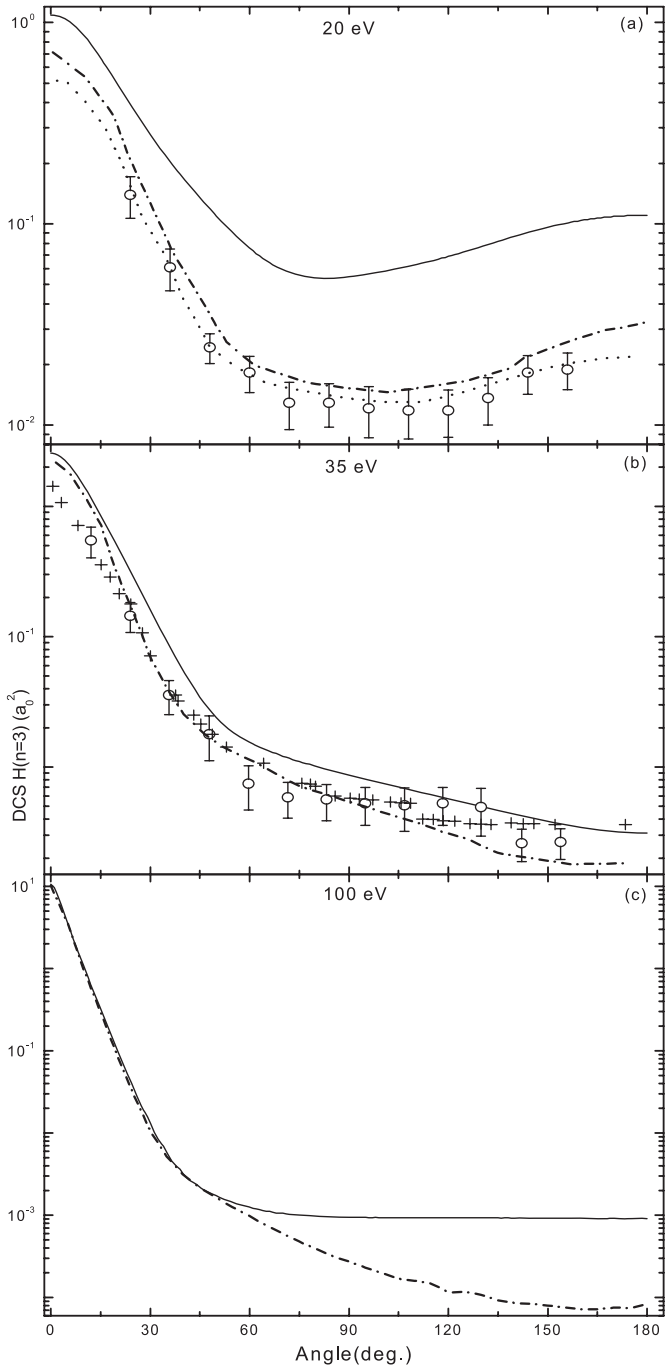

Fig. 5. The DCS for H($1s$) → H($3s + 3p$) excitation at 20, 35 and 100 eV. Theoretical data: similar to Figure 4. Experimental data: (○) Sweeney et al. [33].

that are observed at larger angles. This similar qualitative features can also be seen, in the summed $n = 3$ levels ($3s$+$3p$) (see Figs. 5a–5c). In Figure 5b, at 35 eV, the CCO model is in better agreement with the rest of the theoretical calculations and seems to be within the upper bar of the experimental measurements of Sweeney et al. [33].

3.2 Reduced stokes parameters for 2p and 3p excitation

3.2.1 54.4 eV

The reduced Stokes parameters $\overline{P}_1$, $\overline{P}_2$ and $\overline{P}_3$ for 2p excitation are depicted in Figure 6. In the left-hand columns (Figs. 6a, 6c and 6e), the available experimental and theoretical data are compared among each other, particularly in the region between 0° to 45° scattering angles and in the right-hand columns (Figs. 6b, 6d and 6f), the CCO12, PECS and CC17 are shown with the experimental data [2,23] from 0° to 180°. The CCO9 is not shown in Figure 6 to avoid cluttering, but it must be noted that it shows good convergence with the CCO12. Similarly, the CCC data is also not shown as its agreement with PECS is quite good.

In examining the experimental measurements, it can be seen that the general qualitative trends are demonstrated by nearly all the measurements except in the $\overline{P}_3$ case. Nevertheless, there are quantitative differences between these measurements and the large uncertainties also do not provide a very discriminating description of these parameters at 54.4 eV.

In the $\overline{P}_1$ case (Fig. 6a), there is a clear experimental demonstration that the first minimum appears around the 15°–20° scattering region. However, the experimental data are not discriminating enough to pin-point the actual minima. The theories tend to support this view with the CCO12 showing a clear minima at about 17° and the PECS and CC17 lie in the 15°–16° region. Another observation that has to be noted here is that the present CCO12 shows better agreement with Williams and Mikosza [2] and PECS in this region. This is an important gauge about the quality of the theoretical calculations.

At the forward and middle angles upto about 90° (Fig. 6b), there is a clear two band of theoretical predictions with the CCO12 lying in one band and the PECS and the CC17 in the other. All theoretical data predict a first maxima at around the 45°–55° scattering region and the qualitative trends are supported by the experimental data. At the backward scattering, all theories show different qualitative features suggesting that the scattered wave function using various approximations are sensitive at these angles. The recent measurements seem to support some of these theories in some region or the other. The backward $\overline{P}_1$ parameter is a highly discriminating quantity that can be a critical test of theories and experiments.

The theoretical reduced $\overline{P}_2$ parameter is shown in Figures 6c and 6d. It is quite clear here that the CCO12 differs significantly with the other theories above the scattering angle of 30°. Although the CCO12 shows good agreement with the PECS at the forward angles, its qualitative differences and quantitative disagreement with other theories above 30° is quite glaring! So unlike the PECS and CC17, there seems be an extra minima at about 40°. Nevertheless, it should be noted that the CCO12 show similar qualitative trends with the experimental data [2,23] in the 15°–40° scattering region and closer agreement than any

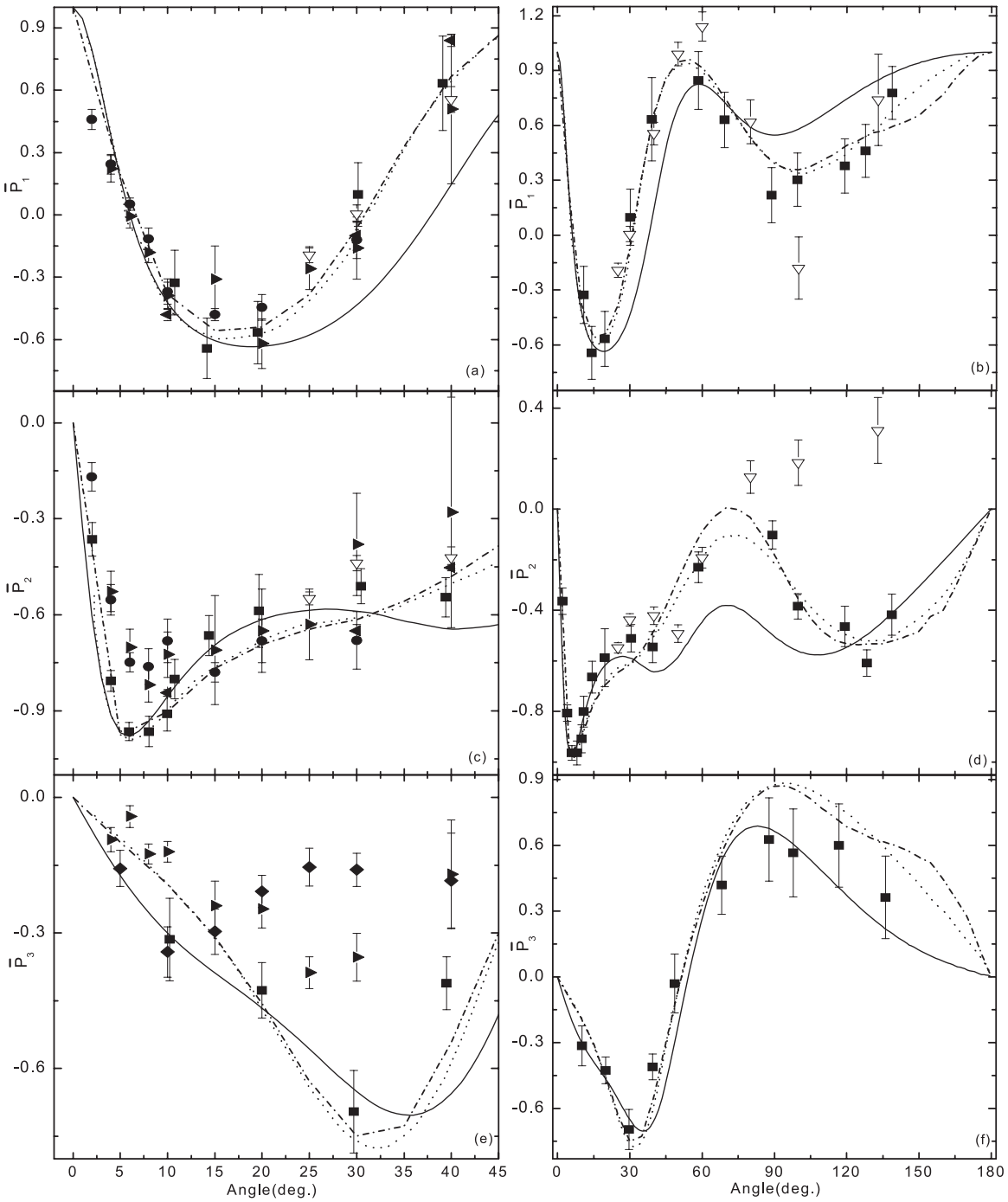

Fig. 6. Reduced Stokes parameters for H($2p$) excitation at 54.4 eV: (a) and (b): $\overline{P}_1$; (c) and (d): $\overline{P}_2$; (e) and (f): $\overline{P}_3$. Legend for PECS, CC17 and CCO12 are as in Figure 1; experimental data: (■) Williams and Mikosza [2], (►) Gradziel and O'Neill [7], (◄) Yalim et al. [10], (●) O'Neill et al. [9], (⧫) Chormaic et al. [25], (▽) Weigold et al. [23].

of the other theoretical data. It should also be noted that the present $\overline{P}_2$ at large scattering angles >120 is closer to the experimental data of Williams and Mikosza [2].

In Figures 6e and 6f, the reduced $\overline{P}_3$ parameter is shown. Overall, qualitative agreement is seen by all theories and the experimental data [2]. The difference with Gradziel and O' Neill [7] and Chormaic et al. [25] experimental data is quite obvious. It seems quite interesting to find that the CCO12 lies within the limits of the Williams and Mikosza's experiment for most angles! However, the backward angles behaviour of the CCO12 continues to show differences with the other theoretical calculations.

The present work was also aimed at studying the $3p$ reduced Stokes parameters. Thus in Figures 7a–7c, the $\overline{P}_1$,

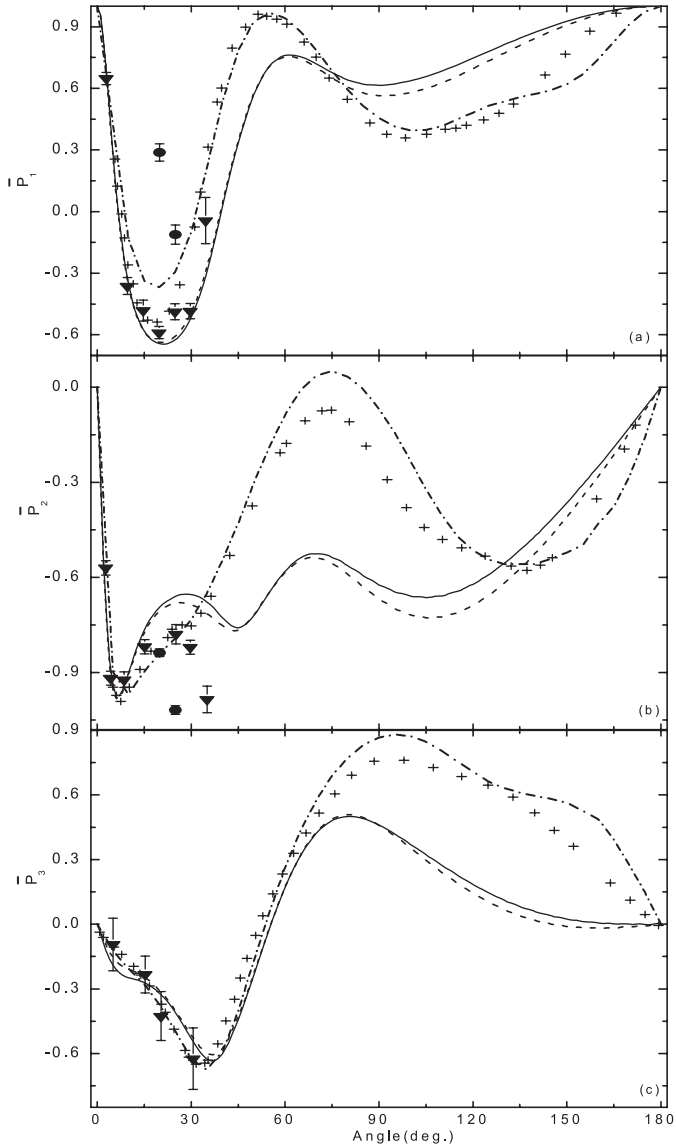

Fig. 7. Reduced Stokes parameters for H(3p) excitation at 54.4 eV: (a) $\overline{P}_1$, (b) $\overline{P}_2$, (c) $\overline{P}_3$. Theoretical data: (——) CCO12, (- - - -) CCO9, (-·-·-) CC17, (+) CCC-L; experimental data: (▼) Williams et al. [29], (●) Chwirot and Slevin [30].

$\overline{P}_2$ and $\overline{P}_3$ parameters are shown with the best available theories and the available experimental data of Williams et al. [29] and Chwirot and Slevin [30]. In the $\overline{P}_1$ case, the present CCO12 and CCO9 show excellent agreement with CCC at the forward angles. At the forward angle and around the first minimum, the present CCO models are showing closer agreement with the experimental measurement of Williams et al. At the backward angles as in the 2p case, the differences between the CCO and the other theoretical data are glaring enough.

As in the 2p excitation, the calculated $\overline{P}_2$ for the 3p excitation by the CCO12 and CCO9 (Fig. 7b) shows quantitative and qualitative differences with the CCC-L and the CC17 above 20° and with all theories showing different qualitative differences at the backward angles. But again, it must be noted that the qualitative trends by the experimental data [29] seems to support the CCO calculations at the 15°–35° scattering region in stark contrast to that of the CCC-L and the CC17 calculations.

Similar conclusions as in $\overline{P}_1$ case can be made for the $\overline{P}_3$ (Fig. 7c).

3.2.2 20 eV, 35 eV and 100 eV

The reduced Stokes correlation parameters $\overline{P}_1$, $\overline{P}_2$ and $\overline{P}_3$ for electron impact excitation of H(2p) and H(3p) at 20, 35 and 100 eV are depicted in Figures 8–10.

In Figure 8a–8c, the theoretical calculations are compared for the reduced Stokes parameters for H(2p) excitation at 20 eV. Although there seems to be an overall qualitative trend among the CCO12, CCO9 and the CC17, there are clear quantitative differences as seen for the $\overline{P}_1$ and $\overline{P}_2$ parameters. The similar difficulties of the CCO models in describing the backward angle scattering DCS at this energy continues to plague the $\overline{P}_1$ and $\overline{P}_2$ data. There is better agreement among theories for the $\overline{P}_3$. The differences between these theoretical calculations are more contrasting for the H(3p) case (see Figs. 8d–8f). It may seem that the CCO is doing severely for the higher excitation process.

The reduced Stokes parameters for the 35 eV excitation of H(2p) and H(3p) are depicted in Figure 9. In Figure 9a, it seems gratifying to find the present CCO calculations are in good qualitative and quantitative accord with the three experimental data points measured at 40 eV by Hood et al. [34] for the $\overline{P}_1$. The CCC-L also shows similar qualitative trend with a deeper minimum at about 20°. However, in the middle and backward scattering angles, the CCO are quantitatively distinct than the CCC-L and CC17. The other experimental measurements by Slevin et al. [35] also do not provide a discerning comparison. Similar comparisons are seen with the $\overline{P}_2$ case at this energy in Figure 9b. In the $\overline{P}_3$ case, there is better agreement among the theories. In Figures 9d–9f, the reduced Stokes parameters for the H(3p) case is shown. There are similarities as well as differences between the theoretical calculations.

The parameters at 100 eV are displayed in Figures 10a–10f. Overall, there is limited agreement between the CCO and the other theoretical data at forward scattering angles as well as with the general trend of the measurements of Hood et al. [34] (2p case) and the Chwirot and Slevin [30] (3p case).

4 Conclusions

In conclusion, the present CCO calculations at 54.42 eV provides a reasonable description of the physics of electron scattering for the $n = 2p$ and 3p excitation. In particular, the calculated DCS are comparable to other *state of the*

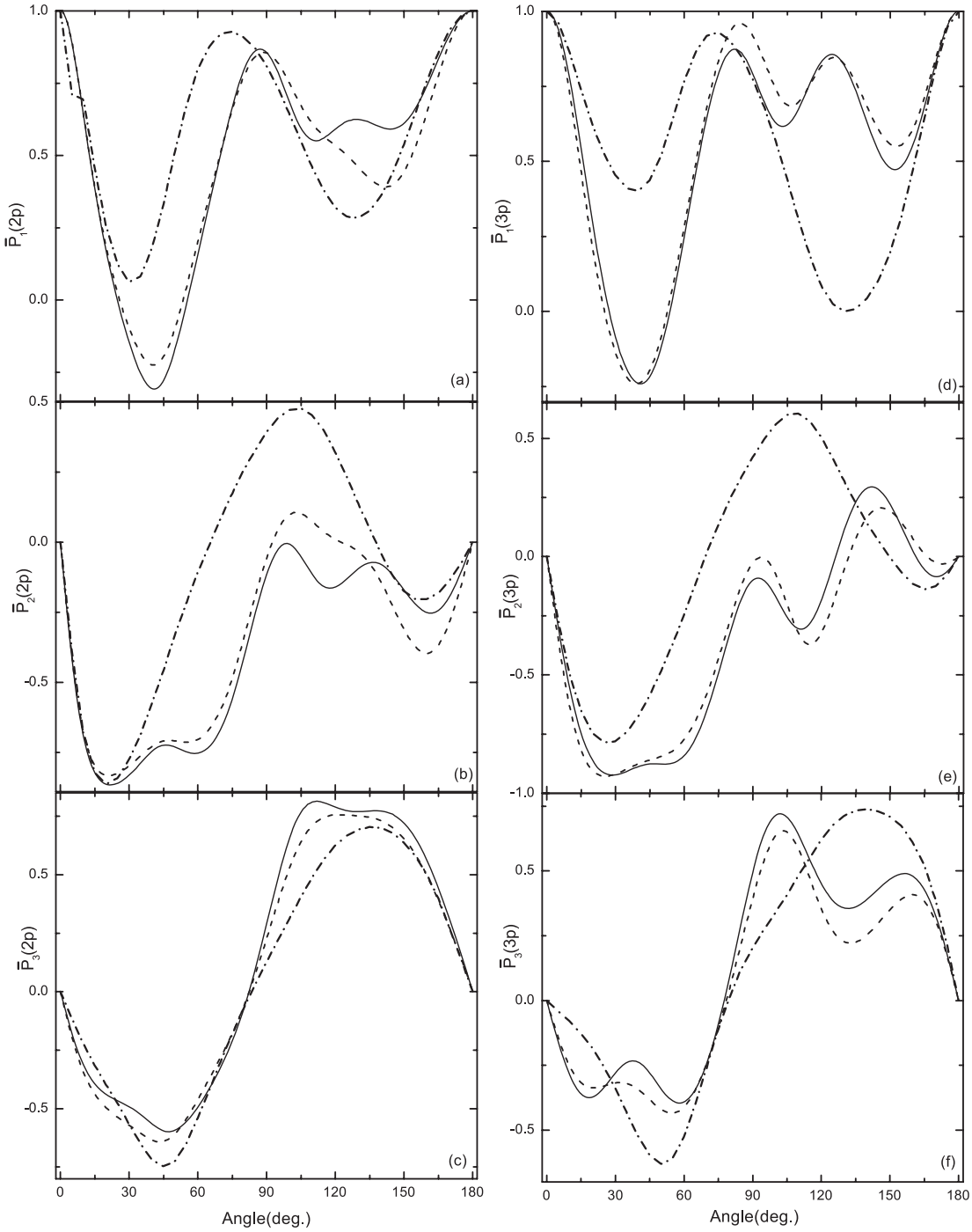

Fig. 8. Reduced Stokes parameters $\overline{P}_1$, $\overline{P}_2$ and $\overline{P}_3$ for H($2p$) and H($3p$) excitation, at 20 eV: legend for CC17, CCO9 and CCO12 are as in Figure 1.

art methods such as the PECS except in the backward scattering region. The CCO calculations also shows limited success for the $n = 3p$ excitation DCS. The plausible explanation of the differences in the middle and backward angles between the CCO and the other theories could be the use of the high-energy approximations in the optical potential model. The differences become less as the energy increases from 20 to 100 eV.

Another physical reason is how well the present theories including the CCO describe the full effects of the direct interaction between the proton and the electron at these larger scattering angles. The exchange approximations used in the calculation of the optical potentials could plausibly affect the CCO models in these large scattering regions.

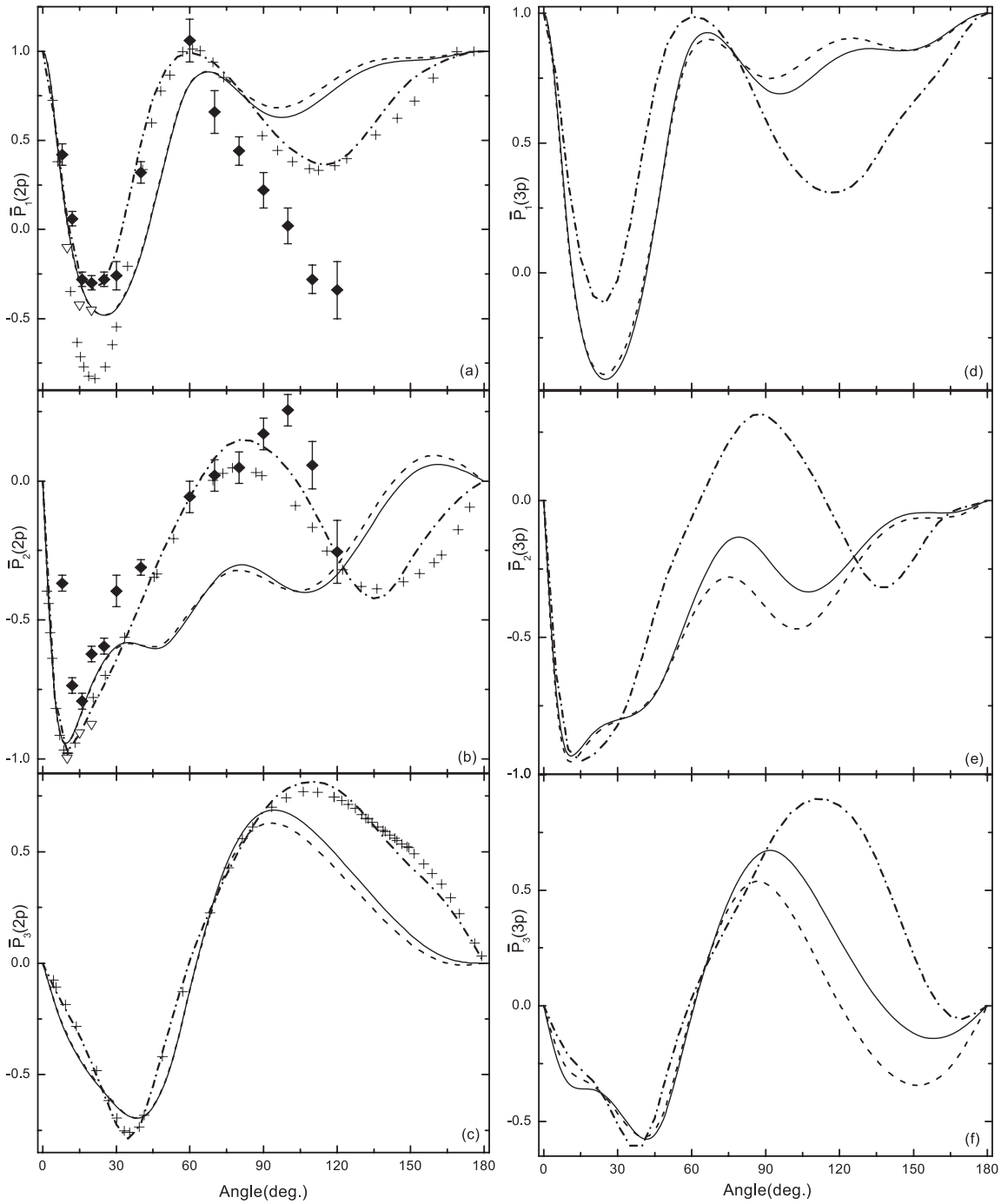

Fig. 9. Reduced Stokes parameters $\overline{P}_1$, $\overline{P}_2$ and $\overline{P}_3$ for H($2p$) and H($3p$) excitation, at 35 eV: legend for CC17, CCC-L, CCO9 and CCO12 are as in Figure 1; experimental data: (♦) Slevin et al. [35], (▽) (40 eV) Hood et al. [34].

In the description of the reduced Stokes parameters for $n = 2p$ and $n = 3p$, the CCO calculation shows only good agreement at forward angles with the PECS and CC17. It must be highlighted that the CCO calculations seem to be in better agreement with the recent measurements of $\overline{P}_1$ by Williams and Mikosza [2] for scattering angles above 120° in the $2p$ excitation of H at 54.42 eV. This is also seen in the $\overline{P}_3$ case where the present CCO12 lies within the limits of the Williams and Mikosza's experimental measurements.

Furthermore, the present CCO calculation is in good accord with the Williams et al.'s experimental measurement of $\overline{P}_1$ and $\overline{P}_3$ [29] for the H($3p$) excitation. Similar qualitative trend with the Williams et al.'s measurement of the $\overline{P}_2$ parameter is reflected in the present CCO work.

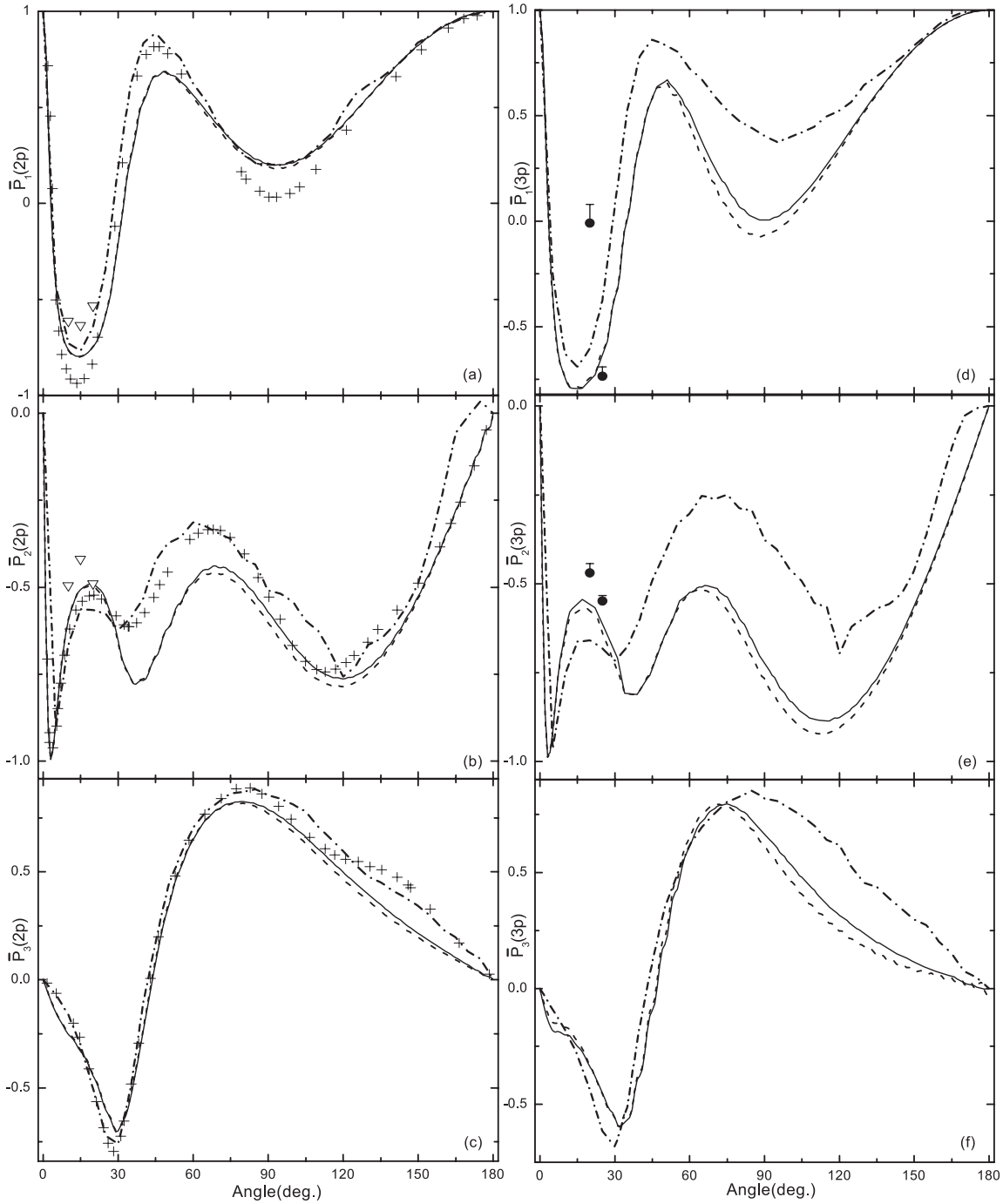

Fig. 10. Reduced Stokes parameters $(\overline{P}_1)$, $(\overline{P}_2)$ and $(\overline{P}_3)$ for H($2p$) and H($3p$) excitation, at 100 eV: legend for CC17, CCC-L, CCO9 and CCO12 are as in Figure 1; experimental data: (•) Chwirot and Slevin [30], (▽) Hood et al. [34].

Nevertheless, in view of the recent PECS calculations, a more discriminating future measurements of the $\overline{P}_1$, $\overline{P}_2$ and $\overline{P}_3$ would help to detail this scattering processes.

KR and MZMK would like to acknowledge the funding from the SAGA grant (No. PHY 35c: Academy of Sciences Malaysia) in fundamental research. ZY also acknowledges support from her research funds.

References

1. P.L. Bartlett, A.T. Stelbovics, G.M. Lee, I. Bray, J. Phys. B **38**, L95 (2005)
2. J.F. Williams, A.G. Mikosza, J. Phys. B **39**, 4113 (2006)
3. K. Ratnavelu, S.Y. Ng, Chin. Phys. Lett. **23**, 1753 (2006)
4. M.Z.M. Kamali, K. Ratnavelu, Phys. Rev. A **65**, 014702 (2002)
5. M.Z.M. Kamali, K. Ratnavelu, J. Fiz. Mal. **27**, 43 (2006)

6. N. Natchimuthu, K. Ratnavelu, Phys. Rev. A **63**, 052707 (2001)
7. M.L. Gradziel, R.W. O'Neill, J. Phys. B **37**, 1893 (2004)
8. K.E. James Jr., J.G. Childers, M.A. Khakoo, Phys. Rev. A **69**, 022710 (2004)
9. R.W. O'Neill, P.J.M. van der Burgt, D. Dziezek, D. Bowe, S. Chwirot, J.A. Slevin, Phys. Rev. Lett. **80**,1630 (1998)
10. H.A. Yalim, D. Cvejanovic, A. Crowe, Phys. Rev. Lett. **79**, 2951 (1997)
11. M.A. Khakoo, M. Larsen, B. Paolini, X. Guo, I. Bray, A.T. Stelbovics, I. Kanik, S. Trajmar, G.K. James, Phys. Rev. A **61**, 012701 (1999)
12. J.F. Williams, P.L. Bartlett, I. Bray, A.T. Stelbovics, A.G. Mikosza, J. Phys. B **39**, 719 (2006)
13. I.E. McCarthy, A.T. Stelbovics, Phys. Rev. A **28**, 2693 (1983)
14. I. Bray, A.T. Stelbovics, Phys. Rev. A **46**, 6995 (1992)
15. Y.D. Wang, J. Callaway, K. Unnikrishnan, Phys. Rev. A **49**, 1854 (1994)
16. I. Bray, K. Bartschat, A.T. Stelbovics, Phys. Rev. A **67**, 060704(R) (2003)
17. T.N. Rescigno, M. Baertschy, W.A. Isaacs, C.W. McCurdy, Science **286**, 2474 (1999)
18. P.L. Bartlett, A.T. Stelbovics, I. Bray, J. Phys. B **37**, L69 (2004)
19. P.L. Bartlett, A.T. Stelbovics, Phys. Rev. A **69**, 022703 (2004)
20. R. Poet, J. Phys. B **13**, 2995 (1980)
21. A. Temkin, Phys. Rev. **126**, 130 (1962)
22. R. Poet, J. Phys. B **11**, 3081 (1978)
23. E. Weigold, L. Frost, K.J. Nygaard, Phys. Rev. A **21**, 1950 (1980)
24. J.F. Williams, J. Phys. B **14**, 1197 (1981)
25. S.N. Chormaic, S. Chwirot, J. Slevin, J. Phys. B **26**, 139 (1993)
26. B. Bederson, L.J. Kieffer, Rev. Mod. Phys. **43**, 601 (1971)
27. N. Andersen, J.W. Gallagher, I.V. Hertel, Phys. Rep. **165**, 1 (1988)
28. N. Andersen, K. Bartschat, *Polarization, Alignment and Orientation in Atomic Collisions* (Springer, 2001)
29. J.F. Williams, A.T. Stelbovics, I. Bray, J. Phys. B **26**, 2165 (1993)
30. S. Chwirot, J. Slevin, J. Phys. B **20**, 6139 (1987)
31. I.E. McCarthy, M.R.C. McDowell, J. Phys. B **12**, 3775 (1979)
32. A. Grafe, C.J. Sweeney, T.W. Shyn, Phys. Rev. A **63**, 052715 (2001)
33. C.J. Sweeney, A. Grafe, T.W. Shyn, Phys. Rev. A **64**, 032704 (2001)
34. S.T. Hood, E. Weigold, A. Dixon, J. Phys. B **12**, 631 (1979)
35. J. Slevin, M. Eminyan, J.M. Woolsey, G. Vassilev, H.Q. Porter, C.G. Back, S. Watkin, Phys. Rev. A **26**, 1344 (1982)